

MESO NUMERICAL STUDY ON THE FAILURE MECHANISM OF ROCK SLOPE WITH BEDDING INTERMITTENT JOINTS

Zhou Yu^{1‡} –Chai Jinfei^{2*‡} –Han Guang^{1,3}

¹ Key Laboratory of Ministry of Education for Efficient Mining and Safety of Metal Mine, University of Science and Technology Beijing 100083, China

² Railway Engineering Research Institute, China Academy of Railway Sciences, Beijing 100081, China

³ China Non-ferrous Metal Mining Group Co., Ltd. Beijing 100029, China

ARTICLE INFO

Article history:

Received: 17.7.2015.

Received in revised form: 18.1.2016.

Accepted: 19.1.2016.

Keywords:

Rock slope

Intermittent bedding joints

Particle flow theory

PFC2D

Meso research

Abstract:

Taking the Muliashi north open-pit mine in Zambia as a case study, the failure mechanism of rock slope with intermittent bedding joints was investigated from a meso mechanical viewpoint using particle flow theory and PFC2D software. In the rock slope model, the rock block and joint were represented by bonded-particle model and smooth-joint model, respectively. The main research results are as follows: (1) Due to orientation and discontinuities of joint, the sliding shape at the bottom of the sliding mass is relatively straight, while the tailing edge shape of sliding mass is flexural and is presenting step-path failure. (2) The fragmented particle assemblies of sliding mass are primarily generated in the middle and bottom part of slope. And they are subsequently generated in the top part of slope. The bulk of fragmented particle assemblies in the middle and bottom part are relatively larger than those in the top part. (3) At the end of sliding process, the contact force of particle is relatively larger along with the direction of rock bridge, and the effect of stress arch is generated around the primary joints. (4) During the sliding process of rock slope, the relationship between the magnitude and count of microseismic events obeys the normal distribution function approximately.

1 Introduction

A rock slope generally consists of structural planes and rock blocks, and its stability and failure mechanism is always an important research subject in slope engineering. Rock slope failure types usually

include circular arc slide, planar slide, fold line slide, wedge slide and toppling failure. The rock slope failure type of my case study is fold line slide. The common analytical methods in rock slope stability analysis include limit equilibrium methods, the finite element method, the finite difference method and the

* Corresponding author. Tel.: +86-13581610996; fax: +86-01062333623

E-mail address: chaijinfei@gmail.com

‡ These authors contributed equally to this work.

discrete element method. Joints can be divided into intermittent joints and persistent joints. The spatial geometric distribution characteristics of joints, which include orientation, angle, spacing, trace length and other related parameters, play an important role in the rock slope stability.

Slope failure is controlled by intermittent joints, and the slope stability is controlled by the rock bridge (that is intact rock strength). Among others, Lisjak and Grasselli [1], Jennings [2], Baczynski [3], Einstein et al [4], Miller et al [5] investigated the calculation method for rock slope with intermittent joints from a theoretical viewpoint. Sagong and Bobet [6] and Prudencio and Van Sint Jan [7] researched the coalescence failure mechanism of rock bridge based on compression tests of jointed rock specimens. Khaira et al analysed the relation between ultrasonic testing and microstructure [8]. However, these research results rarely reveal the failure mechanism of rock slope containing intermittent joints from a meso mechanical viewpoint.

In this paper, the Muliashi north open-pit mine in Zambia is taken as engineering background. Based on the particle flow theory and PFC2D software, rock blocks and joints are represented by a bonded-particle model and a smooth-joint model, respectively. Finally, a simulation model of a rock slope with intermittent bedding joints was created, and the slope characteristics contributing to failure such as microcracks, fragmented particle assemblies, particle contact force and microseismic event, are analyzed in depth from a meso mechanical viewpoint.

2 Case study

The Muliashi north open-pit mine is located in the west part of Luanshya city in Zambia, built in a sedimentary metamorphic copper deposit. The geological and engineering conditions of this open-pit mine are shown in Fig. 1. The exposed stratum in the southern part of the slope consists of different stratum (RL5, RL6 and RL7) with deep roan, containing many bedding planes. The types of rock in all the slopes of Region III are mudstone, quartzite, mica schist and sandstone. The calculation model in this paper is established based on the first stage slope of Region III in Fig. 1, which is only composed of mudstone. The rock mass is broken because its structural planes are development with high degree of weathering.

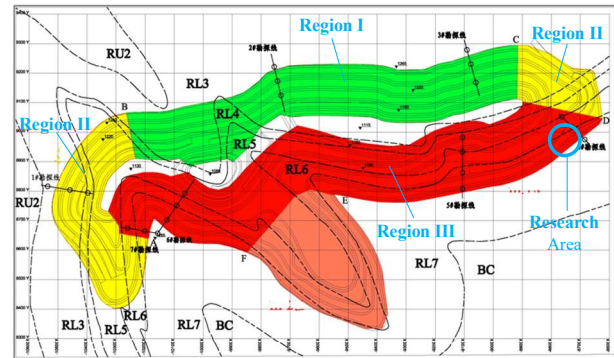


Figure 1. Geologic map of Muliashi north open-pit mine. RU1 is shales and dolomites; RU2 is the layer of argillites; RL3 is the layer of arkose; RL4 is the layer of shale and dolomite; RL5 is the layer of argillite and quartzite; RL6 is the layer of argillite, dolomites and schist; RL7 is the layer of conglomerate, quartzite and argillite; BC is the layer of quartzite, schist and granite.

The research area is located in the eastern part of Region III (the blue circle in the Fig. 1). It exhibits step-path failure (see Fig. 2). The geological survey shows that it is caused by the developed bedding intermittent joints in the rock slope. Since the joints which are perpendicular to the slope surface cannot be established in the two-dimensional model, the cutters are mainly used in the model of this paper.

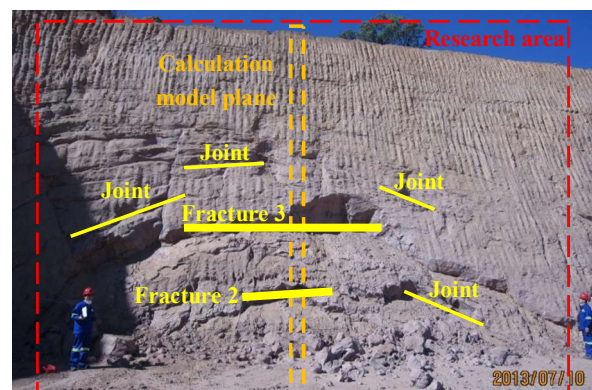


Figure 2. Rock slope conditions

3 Simulation method

The Discrete or Distinct Element Method (DEM) based upon spherical particle basic building-blocks as implemented in the PFC2D software [9,10] is utilized in developing the Equivalent Rock Mass (ERM) [11-12] model. It is worthwhile to mention

that PFC2D simulates the collective behaviour of particles by applying Newton's second law to the particles and a force-displacement law at the contacts. Newton's second law is used to determine the motion of each particle arising from the contact and body forces acting upon it, while the force-displacement law is used to update the contact forces arising from the relative motion at each contact. The collective particle behaviour is obtained numerically using a time-stepping algorithm in which the time-step chosen may be so small that, during a single time-step, disturbances cannot propagate further from any particle than its immediate adjacent particles. Then, at all times, the forces acting on any particle are determined exclusively by its interaction with the particles in contact. Since the speed at which a disturbance can propagate is a function of the physical properties of the discrete system, the time-step can be chosen to satisfy the above constraint. In the simulation presented in this paper, the ERM model is composed of spherical particles interacting through two types of contact force-displacement laws: bonded-particle model (BPM), and smooth-joint model (SJM). The BPM simulates the behaviour of the rock material, while the SJM simulates the behaviour of rock discontinuities. The essential aspects of these contact laws and a list the associated parameters is given in following sub-sections.

3.1 Bonded-particle model

The contact force-displacement laws for bonded-particle implemented in PFC2D, referred to hereafter as BPM, can be considered in three parts: the contact-stiffness model, the bond breakage model, and the slip and separation model. In the simulations performed in this work, linear contact stiffness is used, although nonlinear Hertz-Mindlin type contact stiffness is also available. The parallel bond that approximates the physical behaviour of cement-like substance joining two particles is used for the bond breakage model. Parallel bonds can transmit both force and moment between particles and the bond breakage occurs when the maximum tensile stress exceeds the normal strength ($\sigma_{\max} \geq \bar{\sigma}_c$), or the maximum shear stress exceeds the shear strength ($\tau_{\max} \geq \bar{\tau}_c$) [13]. The maximum tensile and shear stresses acting on the bond periphery are calculated via beam theory to be:

$$\sigma_{\max} = \frac{-\bar{F}^n}{A} + \frac{|\bar{M}_i^s|}{I} \bar{R} \quad (1)$$

$$\tau_{\max} = \frac{|\bar{F}_i^s|}{A} + \frac{|\bar{M}^n|}{J} \bar{R} \quad (2)$$

where smooth-joint radius $\bar{R} = \bar{\lambda} \min(R^{(A)}, R^{(B)})$, with $R^{(A)}$ and $R^{(B)}$ being the particle radii and $\bar{\lambda}$ = the radius multiplier used to set the parallel-bond radii; J = the polar moment of inertia of the parallel-bond cross section. I = the moment of inertia of the parallel-bond cross section.

Furthermore, broken bonds can carry compressive loads and undergo sliding if the contact shear force exceeds the frictional strength. In addition, broken bonds can undergo complete separation as the particles move apart and lose contact.

3.2 Smooth-joint model

The smooth-joint model (SJM) implemented in PFC2D simulates the behaviour of an interface regardless of the local particle contact orientations along the interface [14]. Thus, the behaviour of a joint can be modelled by assigning SJM to all contacts between particles that lie on opposite sides of the joint. The SJM can be envisioned as a set of elastic springs uniformly distributed over a circular cross-section centred at the contact point and oriented parallel with the joint plane as depicted in Fig. 3.

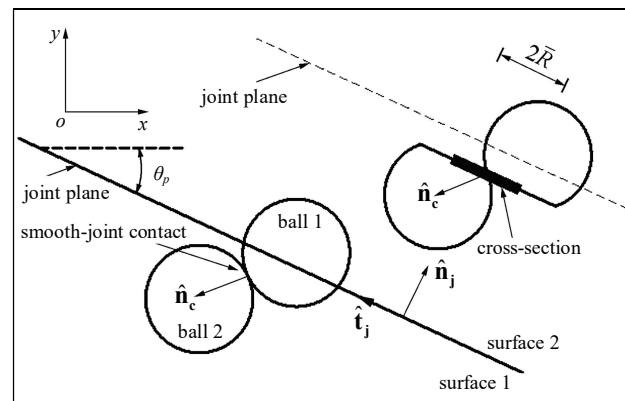


Figure 3. Smooth joint model [9,10]

In this way, the SJM mimics the asperity contacts at a rock joint. The area of the smooth-joint cross section at a contact point is given by:

$$A = \pi \bar{R}^2 \quad (3)$$

$$F_n := F_n + \bar{k}_n A \Delta U_n^e \quad (7)$$

$$F_s' := F_s - \bar{k}_s A \Delta U_s^e \quad (8)$$

where A = the area of the bond disk.

For the SJM, the force and displacements are calculated with respect to the joint plane as follows:

$$\vec{F} = F_n \vec{n} + \vec{F}_s \quad (4)$$

$$\vec{U} = U_n \vec{n} + \vec{U}_s \quad (5)$$

where \vec{U}_s and \vec{F}_s are the displacement and force vector, respectively, that lie in the joint plane, U_n and F_n are the normal force perpendicular to the joint plane, and vector \vec{n} is the outward unit normal vector to the upper surface (surface 2) of the joint plane defined by the dip angle (θ_p) and dip direction (θ_d) as:

$$\vec{n} = (\sin(\theta_p) \sin(\theta_d), \sin(\theta_p) \cos(\theta_d), \cos(\theta_p)) \quad (6)$$

A positive value of U_n denotes overlap while a positive value for F_n denotes compression. When the SJM model is active in PFC2D, the relative displacement increment between the two particles is decomposed into components normal and tangential to the joint surfaces (ΔU_n and ΔU_s) and the total displacement is updated. The incremental force calculation is performed depending upon whether bonded-SJM or unbonded-SJM is specified. In the simulation reported in this paper, unbonded-SJM is used. In this case the elastic portion of the displacement increments (ΔU_n^e and ΔU_s^e) occur while the gap is negative and the SJM force is updated as follows:

Furthermore, if $|F_s'| \leq (F_s^* = \mu F_n)$, μ is the friction coefficient, then $|F_s| = |F_s'|$, otherwise sliding is assumed to occur. During sliding, the following dilatancy law is assumed:

$$\left. \begin{aligned} F_n &:= F_n + [\Delta U_s^* \tan \psi] \bar{k}_n A = F_n + \left(\frac{|F_s'| - F_s^*}{k_s} \right) \bar{k}_n \tan \psi \\ |F_s| &= F_s^* \end{aligned} \right\} \quad (9)$$

where ψ is the dilation angle.

4 Failure characteristics of rock slope with intermittent bedding joints

4.1 Calculation model

The characteristics, such as elasticity modulus, uniaxial compressive strength, Poisson's ratio and density of the mudstone present in the area are 5.96 GPa, 34.5 MPa, 0.15 and 2560 kg/m³, respectively. Cohesion and the friction angle of joints are 149.33 kPa and 12.35°. Based on rock uniaxial compression test and joint direct shear test, the meso mechanical properties of bonded-particle model and smooth-joint model are obtained by varying them until the macro mechanical parameters of the numerical sample matched that of the lab test sample [9,11]. The final meso mechanical parameters are shown in Table 1 and Table 2.

Table 1 Meso mechanical parameters of bonded-particle model

R_{min} /mm	R_a	ρ_{bulk} / (kg/m ³)	μ	E_c / GPa	k_n / k_s	$\bar{\lambda}$	\bar{E}_c / GPa	\bar{k}_n / \bar{k}_s	σ_{n-mean} /MPa	σ_{n-dev} /MPa	τ_{s-mean} /MPa	τ_{s-dev} /MPa
0.50	1.66	2500	0.5	4.8	1.3	1.0	4.8	1.3	23.0	2.3	23.0	2.3

Table 2 Meso mechanical parameters of smooth joint model

sj_kn / (N/m)	sj_ks / (N/m)	sj_fric	sj-da / (°)	sj_bmode	sj_bns / MPa	sj_bcoh /MPa	sj_bfa / (°)
2×10^7	2×10^7	0.2	0	0	0	0	0

In Table 1, R_{\min} is the minimum radius of particle, R_a is the radius ratio between maximum and minimum particle, ρ_{bulk} is the density of particle assemblies, μ is the particle friction coefficient, E_c is the Young's modulus at each particle-particle contact, k_n/k_s is the ratio of particle normal to shear stiffness, $\bar{\lambda}$ is the radius multiplier used to set the parallel-bond radius, \bar{E}_c is the Young's modulus of each parallel bond, \bar{k}_n/\bar{k}_s is the ratio of parallel-bond normal to shear stiffness. $\sigma_{n-\text{mean}}$ and $\tau_{s-\text{mean}}$ are the average value of bond normal and shear strengths, respectively. $\sigma_{n-\text{dev}}$ and $\tau_{s-\text{dev}}$ are the standard deviation of bond normal and shear strengths, respectively.

In Table 2, sj_kn and sj_ks are the joint normal and shear stiffness, respectively, sj_fric is the joint friction coefficient, sj_da is the joint dilation angle, sj_bmode is the joint bond mode, sj_bns is the joint bond normal (tensile) strength, sj_bcoh is the joint bonded system cohesion, sj_bfa is the joint bonded system friction angle.

Based on slope design information and field geological survey data, the meso analysis model of rock slope with intermittent bedding joints is constructed (see Fig. 4, bedding intermittent joints are based on the boreholes and rock mass classification). The actual width and height of the slope are 30 m and 22.5 m, respectively. The slope bench and angle are 15 m and 65°, respectively. Because the focus of this research is on the slope failure pattern and the influence of height at bottom is very small [15], so, this model is terminated 7.5 m on the right plateau. Based on analysis results of field joint, smooth-joint model is used to construct the parallel intermittent joints in slope. The sediment consists of five layers, which are sorted from bottom to top. The length and orientation (dip angle) of each joint is 3 m and 25°, respectively. The horizontal distance of each joint in the same layer is 3 m, and the perpendicular distance between adjacent two layers is 2.14 m. Due to the small impact of lower joint on the slope stability, only the intermittent joints above the slope toe are constructed.

The minimum particle radius in the slope model is 8×10^{-2} m, and the number of particles is 12325. The displacement in the x direction is fixed on the left and right boundary; the displacement in x and y directions is fixed on the bottom boundary; and the displacement in x and y directions is unfixed on the

highest point of the model. In order to reproduce the slope failure, the particle density is increased starting from 2560 kg/m³ until the rock slope starts to fail. In the process of slope failure simulation, the density is increased 10 times up to 25600 kg/m³.

Based on the meso analysis, the model of rock slope is shown in Fig. 4, and the failure characteristics of rock slope with intermittent bedding joints such as microcracks, fragmented particle assemblies, particle contact force and microseismic event, are further researched from meso mechanical viewpoint.

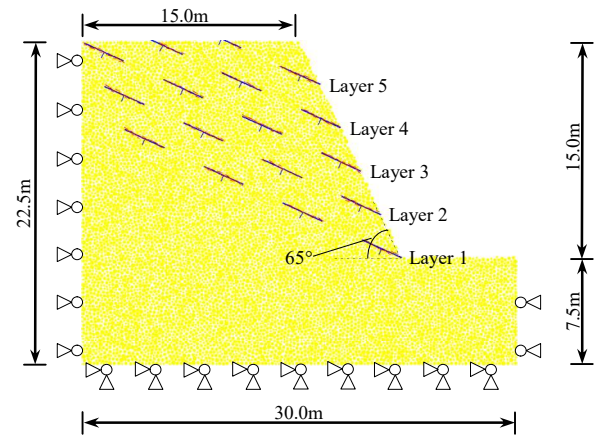


Figure 4. Meso analysis model of rock slope

4.2 Calculation results

The space-time propagation of microcracks during the sliding process of rock slope is shown in Fig. 5. The tensile and shear microcrack are represented by red and black short line. Calculation results show that the microcracks have the following characteristics: (1) The unfavourable orientation of discontinuities is determined by primary joints and fractures. The microcracks are generated between intermittent joint endpoints in the rock, and mostly under the joint length. (2) Microcracks start to generate at the joint endpoint at the bottom bench, and develop towards the upper part of the slope. (3) The unfavourable orientation of discontinuities at the bottom is relatively straight, and it consists of primary joints and microcracks generated between joint endpoint in the same layer. (4) Due to the microcracks formation inside the rock bridge, the failure in this intact rock is expected along the microcrack planes. The flexural formation of microcracks is visible, but that doesn't necessarily

imply on sliding mass border. The microcrack planes present step-path failure, and it consists of primary joint and microcracks generated between joint endpoint in the adjacent layers.

The space-time evolutionary characteristic of fragmented particle assemblies during the sliding process of the rock slope is shown in Fig. 6. The computed result of rock slope failure type in my case study is fold line slide. The fragmented particle assemblies represent the intact rock blocks which break away from rock mass on the slope (tension failure) due to the generation of microcracks. The single fragmented particle assembly consists of many circular particles and the bonds between these particles are not destructive. In Fig. 6, different fragmented particle assemblies are represented by different colour entities.

At the end of step 10000, fragmented particle assemblies presenting wedge-shape start to be generated from the primary joints of the slope. At the end of step 17500, the scope of fragmented particle assemblies extends from middle to bottom part of the slope. At this time, the top part of slope is undamaged. At the end of step 20000, fragmented particle assemblies start to generate at

the top part of slope, and their bulks are larger than those at the middle and bottom part of slope. At the end of step 22500, the fragmented particle assemblies is further fail from big bulks to small bulks due to the sliding process of the slope.

The contact force distribution between particles in the beginning and in the end of simulation is shown in Fig. 7. The contact force distribution near slope surface is approximately parallel to slope surface before sliding initiation, and this status is similar to uniaxial compression condition (Fig. 7(a)). When the position is away from slope surface, the contact force gradually returns to initial stress state, and the vertical component of the in situ stress is larger than horizontal component.

In Fig. 7(b), after sliding process, the contact force along with rock bridge direction is relatively larger, and this phenomenon is obvious at the bottom part of the slope. Near the joint surface, the contact force is relatively small, however, away from joint surface, the contact force gradually increases. Finally, the effect of stress arch generates around joint after sliding process. Due to this, microcracks are mainly generated along with the direction of rock bridges during landslide. And microcracks are also generated in the area of joints.

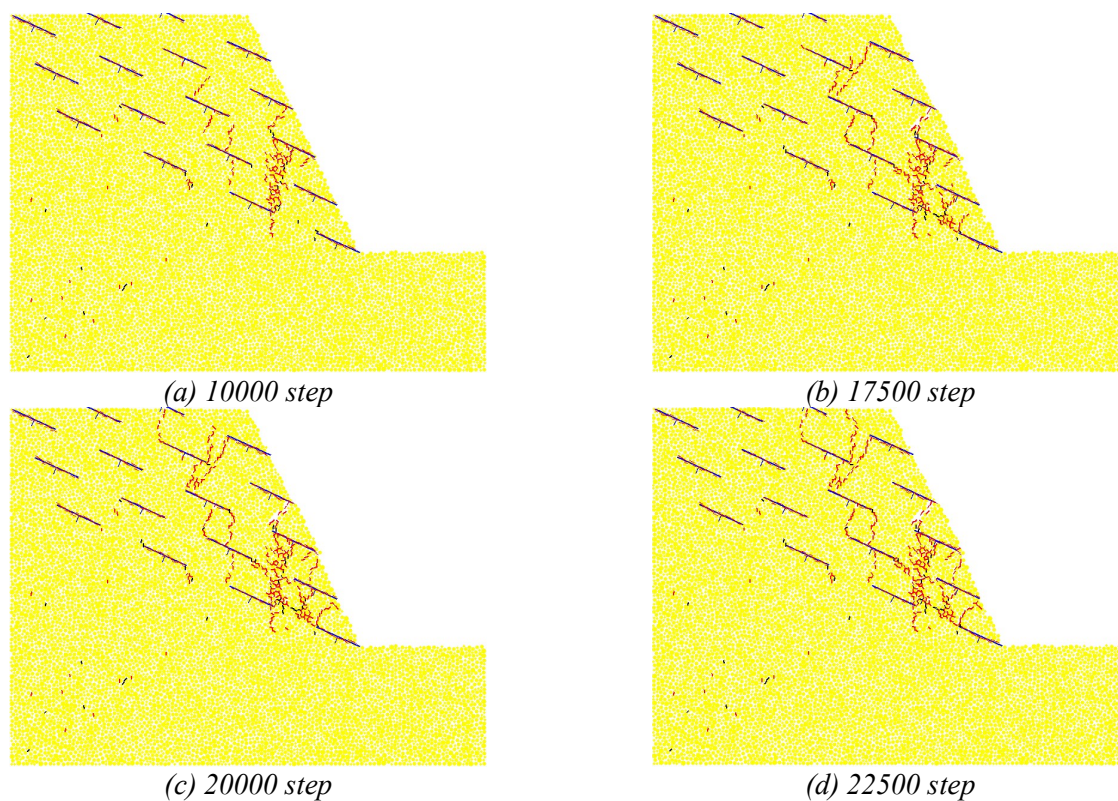


Figure 5. Propagation and position of microcracks in the jointed rock mass

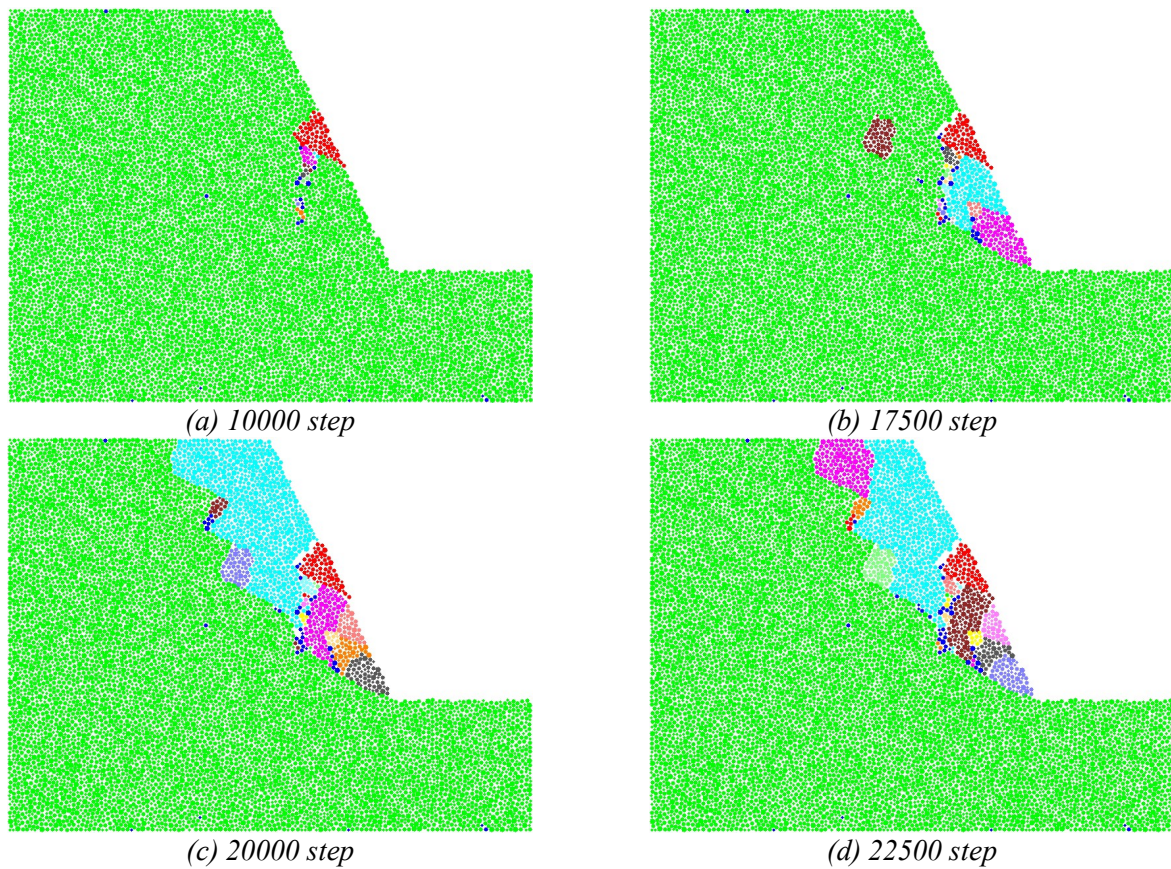


Figure 6. Evolutionary process of fragmented particle assemblies

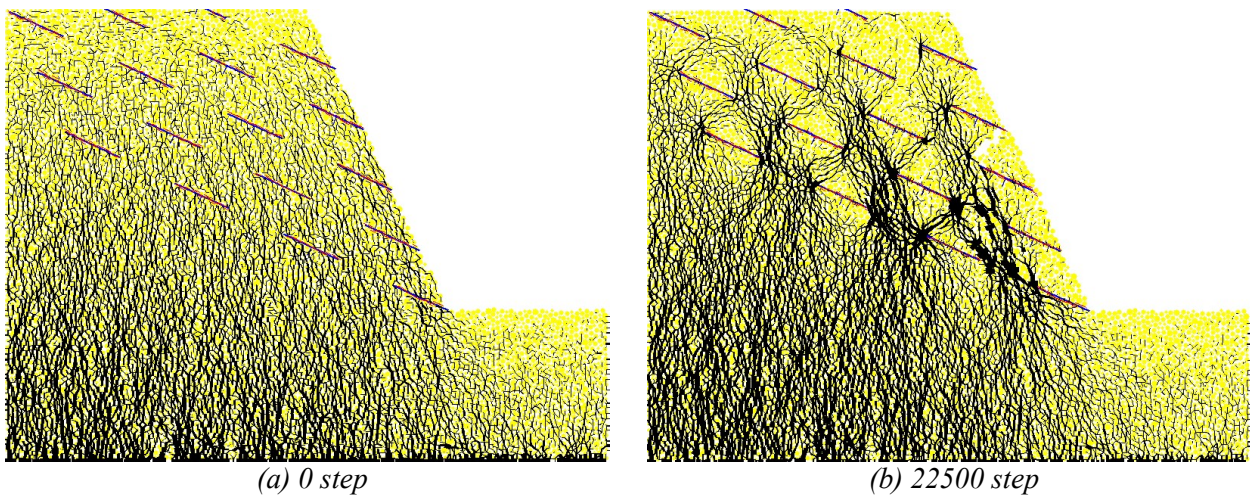
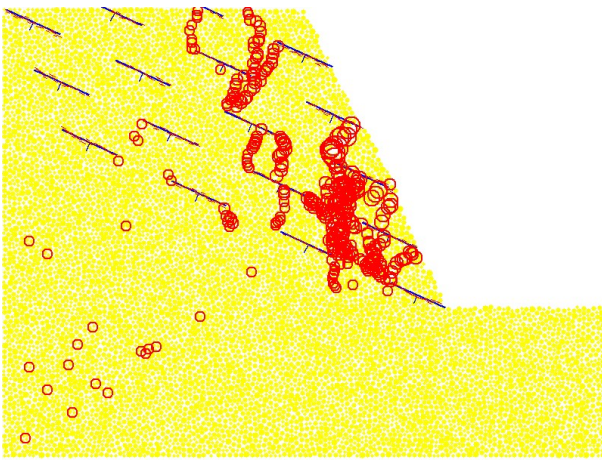


Figure 7. Contact force distribution between particles

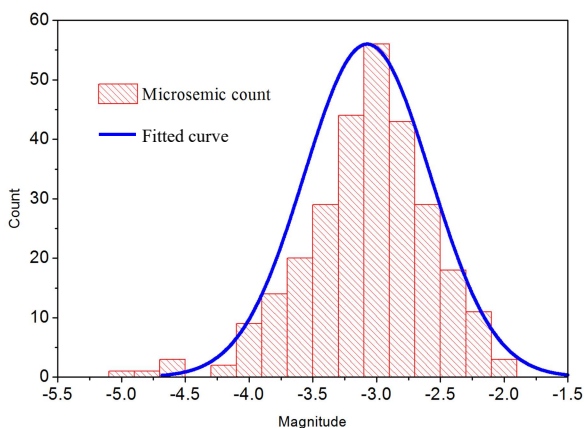
At the end of step 22500, the distribution of microseismic events and the relationship between magnitude and count (number) of microseismic are shown in Fig. 8, in which the circle centre and size represent the location and magnitude of microseismic event, respectively. The following

comments can be made based on the calculation results:

The relationship between the magnitude and number of microseismic events approximately satisfies the Gaussian distribution function, and the mean value and standard deviation of the magnitude are -3.07 and 0.495, respectively.



(a) Distribution of microseismic events. The microseismic events are mainly generated from the middle to the bottom part of the slope, and their density and magnitude are relatively larger than the microseismic events at top part of slope



(b) Relationship between microseismic magnitude and count (number). The calculation results show that the amount of microseismic events throughout the sliding process of the slope is 238 and the maximum and minimum magnitude of microseismic events are -2.05 and -4.91, respectively.

Figure 8. Characteristics of microseismic events (22500step)

5 Discussion and Conclusion

Hazzard and Young [16,17], Zhou et al [18] and Wang et al [19] established the simulative approach of rock acoustic emission (AE) in meso-scale by using the moment tensor theory. This

approach can simultaneously give the occurrence characteristics of AE event such as time, location and magnitude by calculating the moment tensor based on the change contact force when bonds are damaged.

In this paper, the Muliashi north open-pit mine in Zambia is taken as engineering background. The failure mechanism of rock slope with intermittent bedding joints was investigated from meso mechanical viewpoint using particle flow theory and PFC2D software. The main research results are:

(1) Due to orientation and discontinuities of joint, the sliding shape is relatively straight at the bottom of the sliding mass. The microcrack planes present a step-path failure. They are generated between the primary joints endpoint in the same layer, and generated along the joint length. Due to the formation of microcracks inside the rock bridge, the failure in this intact rock is expected along the microcrack planes. The flexural formation of microcracks is visible, but it doesn't necessarily imply that those microcracks are located on sliding mass border.

(2) The fragmented particle assemblies of sliding mass are primarily generated in the middle and bottom part of slope. And they are subsequently generated in the top part of the slope. The bulk of fragmented particle assemblies in the middle and bottom part are relatively larger than those in the top part.

(3) At the end of sliding process, the contact force of particle is relatively larger along with the direction of Rock Bridge, and the effect of stress arch is generated around the primary joints.

(4) During the sliding process of rock slope, the relationship between the magnitude and number of microseismic events obeys the normal distribution function approximately.

In summary, the research method and conclusion can overcome the deficiency of existing theory, lab test and numerical simulation, and function as a beneficial reference to investigate the failure mechanism of jointed rock slope systematically.

Acknowledgements

This research is supported by the National Natural Science Foundation of China (No. 51504016), China Postdoctoral Science Foundation (No. 2015M570037) and Fundamental Research Funds for the Central Universities (No. FRF-TP-15-036A2).

References

- [1] Lisjak, A., Grasselli, G.: A review of discrete modelling techniques for fracturing processes in discontinuous rock masses, *Journal of Rock Mechanics and Geotechnical Engineering*, 2014, 6(4), 301–314.
- [2] Jennings, J. E.: A mathematical theory for the calculation of the stability of slopes in open cast mine, *Proceedings of the Symposium on Planning Open Pit Mines*, Johannesburg, 1970, 87-102.
- [3] Baczynski, N. R. P.: STEPSIM4 “step-path” method for slope risks, *International Conference on Geotechnical and Geological Engineering*, Australia, 2000, 86-92.
- [4] Einstein, H. H., Veneziano, D., Baecher, G. B.: The effect of discontinuity persistence on rock slope stability, *Journal of Rock Mechanics and Mining Science and Geomechanics Abstracts*, 1983, 20(5), 227-236.
- [5] Miller, S., Whyatt, J., McHugh, E.: Applications of the point estimation method for stochastic rock slope engineering, *Gulf Rocks 2004: Proceedings, Rock Mechanics Across Borders and Disciplines*, 6th North American Rock Mechanics Conference, Houston Texas, ARMA/NARMS (04-517).
- [6] Sagong, M., Bobet, A.: Coalescence of multiple flaws in a rock-model material in uniaxial compression, *International Journal of Rock Mechanics and Mining Sciences*, 2002, 39(2), 229-241.
- [7] Prudencio, M., Van Sint, J. M.: Strength and failure modes of rock mass models with non-persistent joints, *International Journal of Rock Mechanics and Mining Sciences*, 2007, 44(6), 890-902.
- [8] Khaira, A., Srivastava, S., Suhane, A.: Analysis of relation between ultrasonic testing and microstructure: a step towards highly reliable fault detection, *Engineering Review*, 35(2), 87-96, 2015.
- [9] Itasca Consulting Group: PFC2D (Particle Flow Code in 2 Dimensions) Theory and Background, Itasca, USA: Itasca Consulting Group, 2008.
- [10] Itasca Consulting Group: PFC2D (Particle Flow Code in 2 Dimensions) FISH in PFC2D, Itasca, USA: Itasca Consulting Group, 2008.
- [11] Zhou, Y., Wu, S. C., Wang, L.: Application of equivalent rock mass technique to mesoscopic analysis of fracture mechanism of rock specimen containing two intermittent joint. *Rock and Soil Mechanics*, 2013, 34 (10), 2801-2809.
- [12] Zhou, Y., Wu, S. C., Gao, Y. T. et al: Meso-research on mechanical properties of rock mass affected by joint connectivity rate *Rock and Soil Mechanics*, 2015, 36 (2), 29-36.
- [13] Potyondy, D. O., Cundall, P. A.: A bonded-particle model for rock, *International Journal of Rock Mechanics and Mining Sciences*, 2004, 41(8), 1329-1364.
- [14] Scholtes, L., Donze, F. V.: Modelling progressive failure in fractured rock masses using a 3D discrete element method, *International Journal of Rock Mechanics and Mining Sciences*, 2012, 49(1), 18-30.
- [15] Wang, C., Tannant, D. D., Lilly, P. A.: Numerical analysis of the stability of heavily jointed rock slopes using PFC2D. *International Journal of Rock Mechanics & Mining Sciences*, 2003, 40, 415-424.
- [16] Hazzard, J. F., Young, R. P.: Simulating acoustic emissions in bonded-particle models of rock, *International Journal of Rock Mechanics and Mining Sciences*, 2000, 37(5), 867-872.
- [17] Hazzard, J. F., Young, R. P.: Moment tensors and micromechanical models, *Tectonophysics*, 2002, 356 (1/3), 181-197.
- [18] Zhou, Y., Wu, S. C., Xu, X. L.: Particle flow analysis of acoustic emission characteristics during rock failure process, *Chinese Journal of Rock Mechanics and Engineering*, 2013, 32(5), 951-959.
- [19] Wang, L., Tan, Z. Y., Zhou, Y.: Mesoscopic simulative research on acoustic emission characteristic of coal sample in Brazilian test, *Journal of University of Science and Technology Beijing*, 2014, 36 (3), 275-282.